

VISCOELASTIC LID-DRIVEN CAVITY FLOWS

P. J. Oliveira

Departamento de Engenharia Electromecânica
Unidade de Materiais Têxteis e Papeleiros
Universidade da Beira Interior
6201-001 Covilhã
e-mail: pjpo@ubi.pt, web: <http://www.ubi.pt>

Key words: Cavity Flow, Viscoelastic, FENE-CR, Elastic Recoil, Finite-Volume

Abstract. *Viscoelastic flow in a square cavity is studied in detail for the FENE-CR model with a given value of extensibility. A finite volume method was employed to predict both the steady flows resulting from movement of the top cavity wall and also the recoil flows that follow the cessation of that lid-wall motion, when the fluid possesses viscoelastic properties. It is shown that this recoil flow can be captured by simple elastic models based on finite extensibility and that the steady flow in the cavity can be predicted for relatively high elasticity values, provided the lid-driven wall velocity is regularised.*

1. INTRODUCTION

Cavity flows driven by the tangential movement of one of the walls are prototypical recirculating flows in computational fluid dynamics studies and have been the focus of interest for almost 40 years, starting with the pioneering paper by Burggraaf in 1966. Most of the interest has been purely theoretical and has resided on the possibility of having a complex flow pattern in a very simple geometry, with the level of complexity augmenting as the Reynolds number is increased, for Newtonian fluids. However, the cavity geometry serves also practical purposes as it mimics, for example, the processes occurring in coating devices.

Lid-driven cavity flows with non-Newtonian viscoelastic fluids have received less attention, but still some experimental [1] and theoretical [2] works can be found in the literature. Again, the simple geometry offers the promise of using the cavity as a convenient benchmark test-flow in computational rheology. The main problem associated with this kind of numerical simulations is related to the level of stress growth near the corners between the lid and the side walls. Due to those singularities (see [2]), the attainable Deborah numbers (De) are very low for the original un-regularized cavity (De around 0.20, see [3]), a feature that may explain the lack of interest for this flow. In the present work the cavity is regularized by prescribing a polynomial velocity profile which goes to zero at the corners, hence avoiding discontinuous velocities on the cavity boundary. We present results for De up to 10, under conditions of negligible inertia (creeping flow more typical of non-Newtonian high-viscosity liquids, $Re = 0$). In addition, we consider the recoil process that follows the cessation of the lid movement, which was visualized with PIV in the experimental work of Pakdel et al. [1]. We employ the FENE-CR model to represent the rheology of a viscoelastic Boger fluid, and show that the recoil is captured by the time dependent simulations, starting with $De = 4$. Where possible, the results are compared with the data of Ref. [1].

2. EQUATIONS

We are concerned with the flow of polymer solutions, formed by a Newtonian solvent (subscript s) and an elastic polymer solute (subscript p), in a square two-dimensional cavity. Using standard notation, the mass and momentum equations are:

$$\frac{\partial \mathbf{r}}{\partial t} + \tilde{\mathbf{N}} \cdot (\mathbf{r}\mathbf{u}) = 0 \quad (1)$$

and

$$\left(\frac{\partial (\mathbf{r}\mathbf{u})}{\partial t} + \tilde{\mathbf{N}} \cdot (\mathbf{r}\mathbf{u}\mathbf{u}) \right) = -\tilde{\mathbf{N}}p + \tilde{\mathbf{N}} \cdot \mathbf{t}_s + \tilde{\mathbf{N}} \cdot \mathbf{t} \quad (2)$$

to be solved for the pressure p and the velocity vector \mathbf{u} . The rheological equation for the Newtonian solvent is

$$\mathbf{t}_s = 2\mathbf{h}_s \mathbf{D} = 2\mathbf{h}_s \frac{1}{2} (\tilde{\mathbf{N}}\mathbf{u} + \tilde{\mathbf{N}}\mathbf{u}^T) \quad (3)$$

and for the elastic part of the stress we employ a form of the FENE-CR model (Chilcott and Rallison [4]):

$$\mathbf{t} + \mathbf{I}_{eq} \left(\frac{\partial \mathbf{t}}{\partial t} + \tilde{\mathbf{N}} \cdot (\mathbf{u}\mathbf{t}) \right) = \mathbf{h}_p (\tilde{\mathbf{N}}\mathbf{u} + \tilde{\mathbf{N}}\mathbf{u}^T) + \mathbf{I}_{eq} (\mathbf{t} \cdot \tilde{\mathbf{N}}\mathbf{u} + \tilde{\mathbf{N}}\mathbf{u}^T \cdot \mathbf{t}) \quad (4)$$

This last equation is solved for the polymeric component of the stress tensor \mathbf{t} , while the solvent component is substituted directly into the momentum equation and dealt with implicitly. Both viscosity coefficients are assumed constant, giving a total fluid viscosity of $\mathbf{h}_0 = \mathbf{h}_s + \mathbf{h}_p$ with solvent proportion fixed by $\mathbf{b} = \mathbf{h}_s / \mathbf{h}_0$, and density \mathbf{r} is also constant (incompressible flow). An equivalent relaxation time (\mathbf{I}) is defined as

$$\mathbf{I}_{eq} = \mathbf{I} / f(\mathbf{t}) \quad (5)$$

and varies with the trace of the elastic stress according to the expression

$$f(\mathbf{t}) = \frac{L^2 + \frac{\mathbf{I}}{\mathbf{h}_p} tr(\mathbf{t})}{L^2 - 3} \quad (6)$$

where L^2 is a parameter of the FENE-CR model related to its extensional properties. If a polymer molecule can be extended by a large margin in relation to its equilibrium value, then L^2 is large; typical values lie in between 100 and 1000. When L^2 goes to infinity, the above model tends to the well-known Oldroyd-B model, which has the problem of unbounded extensional viscosities at finite rates of extension.

3. NUMERICAL METHOD

A finite volume formulation already presented and discussed in a number of previous publications [5;6] is employed to solve the set of differential equations given in Section 2. Basically, the equations are integrated over a time step and over a spatial control volume, with the main variables stored at the centre of these cells forming the computational mesh, interpolation formulae are used to

approximate derivatives and calculate variables in positions where they are not stored, and sets of apparently linear, algebraic equations are obtained. These are solved with standard methods of linear algebra, namely conjugate-gradient type of solvers. All this is quite well-known and there is no need to repeat the details here. We just give the equations in discretised form so that the inter-relations among them become clear.

Integration of the time derivative terms is made through the approximation [5]:

$$\frac{\partial \mathbf{f}}{\partial t} \approx \frac{(1+\mathbf{k})\mathbf{f}^{n+1} - (1+2\mathbf{k})\mathbf{f}^n + \mathbf{k}\mathbf{f}^{n-1}}{\Delta t} \quad (7)$$

where \mathbf{f} refers to any of the unknown variables, Δt is the time step and \mathbf{k} is equal to $\frac{1}{2}$ for a second-order scheme.

Considering that density is constant, the mass equation after integration becomes a balance of mass fluxes entering and leaving any of the control volumes forming the mesh through their faces (denoted by f):

$$\sum_f F_f = 0 \quad (8)$$

where the summation is over the 4 faces (2D application). We note that a fully-implicit procedure is adopted, so all variables without a superscript are assumed to be evaluated at the next time level, denoted $n+1$, while the present time is n . The discretised momentum equation is written as

$$a_p \mathbf{u}_p = \sum_F a_F \mathbf{u}_F + S(\tilde{N}p) + S_{HRS}(\mathbf{u}) + S(\mathbf{t}) + S(\mathbf{u}_p^n) \quad (9)$$

where a_F are convection/diffusion coefficients, a_p is the central coefficient made up by the sum of adjacent coefficients and an inertial term, and the other terms S on the rhs are treated as “source” terms. These are the similar to the “constant” terms in a linear system of equations, $Ax = b$, evaluated with existing variable values, i.e. those from a previous iteration.

Similarly, the constitutive equation of the FENE-CR model is discretized as

$$a_p^t \mathbf{t}_p = \sum_F a_F^t \mathbf{t}_F + S_{HRS}^t(\mathbf{t}) + S^t(\mathbf{t}, \tilde{N}\mathbf{u}) + S^t(\mathbf{t}_p^n) \quad (10)$$

and an important difference with the momentum equation is that the coefficients have only convective contributions. A further requirement for the method to be second-order accurate is that the

convective scheme needs to have higher order accuracy. For this, the CUBISTA scheme developed by Alves et al [6] was employed which essentially relies on the use of the following approximation for a convected variable:

$$\tilde{f}_f = \text{Max} \left\{ \tilde{f}_p, \text{Min} \left[\frac{7}{4} \tilde{f}_p, \frac{3}{8} + \frac{3}{4} \tilde{f}_p, \frac{3}{4} + \frac{1}{4} \tilde{f}_p \right] \right\} \quad (11)$$

where f represents any variable (velocity or stress component), f denotes its face value and \tilde{f} a non-dimensional value for f ($\tilde{f} = (f - f_p) / (f_F - f_p)$) where P and F denote consecutive cells along the flow direction; see [6]).

4. PROBLEM DESCRIPTION AND MESHES

Figure 1 shows a sketch of the flow geometry for the lid-driven cavity problem. The top wall moves to the right either with a constant speed U_w (as in the experiments of [1]) or with a variable velocity profile given by:

$$U(x) = U_w 16x^2(1-x)^2 \quad (12)$$

This profile was previously used by [7] and allows a regularisation of the two singular corners marked with black dots in Fig. 1. The cavity has a width of L and height H ; for a square cavity, $L = H$, and the Weissenberg and Deborah numbers coincide (see [1]):

$$De = \frac{IU_w}{H} \quad (13)$$

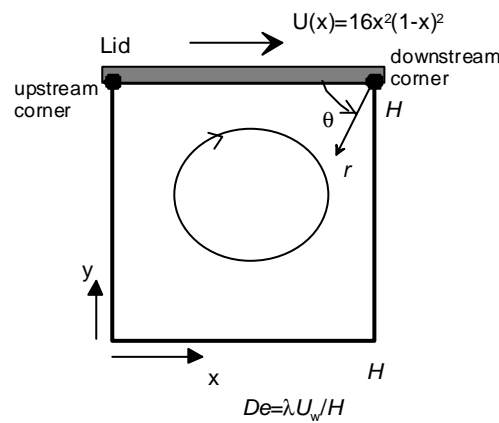


Figure 1. Sketch of the flow geometry.

To obtain non-dimensional variables which will be used throughout from now on, distances will be scaled with the cavity height H , velocities with the maximum cavity speed U_w , time with a convective time scale H/U_w , and pressure and stresses with $\mathbf{h}_0 U_w / H$. The relevant non-dimensional groups are the Deborah number, defined above, the Reynolds number, $Re = \mathbf{r} U_w H / \mathbf{h}_0$, which will be taken as zero in most simulations ($Re = 0$) since inertial effects are very small in most experiments involving polymer melts or solutions in cavities, and an elasticity number defined as:

$$E = \frac{\mathbf{h}_0 l}{\mathbf{r} H^2} \quad (14)$$

It is noted that E is the ratio of the relaxation time, characterising the elastic properties of the fluid, and a diffusion time scale $t_D = H^2 / (\mathbf{h}_0 / \mathbf{r})$. In addition, there are two non-dimensional parameters related to the rheology model: the extensibility parameter L^2 and the solvent viscosity ratio \mathbf{b} . Following the recommendations of [1] who have also tried to fit the properties of the polymer solution of their experiments with the FENE-CR model, we have used:

$$L^2 = 100 \quad \text{and} \quad \mathbf{b} = 0.79 \quad (15)$$

Various meshes have been employed in the simulations with increasing levels of resolution so that a measure of the discretisation error involved could be extracted. Table 2 provides the main characteristics of the meshes used in the study. Most simulations were based on mesh 160 NU (non-uniform) shown in Fig. 2, together with mesh 100 NU; notice that in the former mesh the central core of the cavity, $0.1 \leq x, y \leq 0.9$, is covered with a 100x100 uniform sub-mesh. Some cases, basically for the purpose of performing accuracy tests, were based on meshes with 50x50 and 200x200 uniform spacing, composed after Grid 2 of Table 1. Furthermore meshes 50x50 NU and 200x200 NU non-uniform spacing were patterned after Grid 3.

Grid	Type	Numb. Cells	Min./Max cell spacing, Δx	Cell expansion factor, f_x	Δt
1	40x40 U	1,600	0.025	1.0	0.0025
2	100x100U	10,000	0.01	1.0	0.001
3	100x100 NU	10,000	0.001/0.036	1.0761	0.001/0.0005
4	160x160 NU	25,600	0.001/0.008	1.0732	0.001

Table 1. Main characteristics of computational meshes (U- uniform; NU- non-uniform).

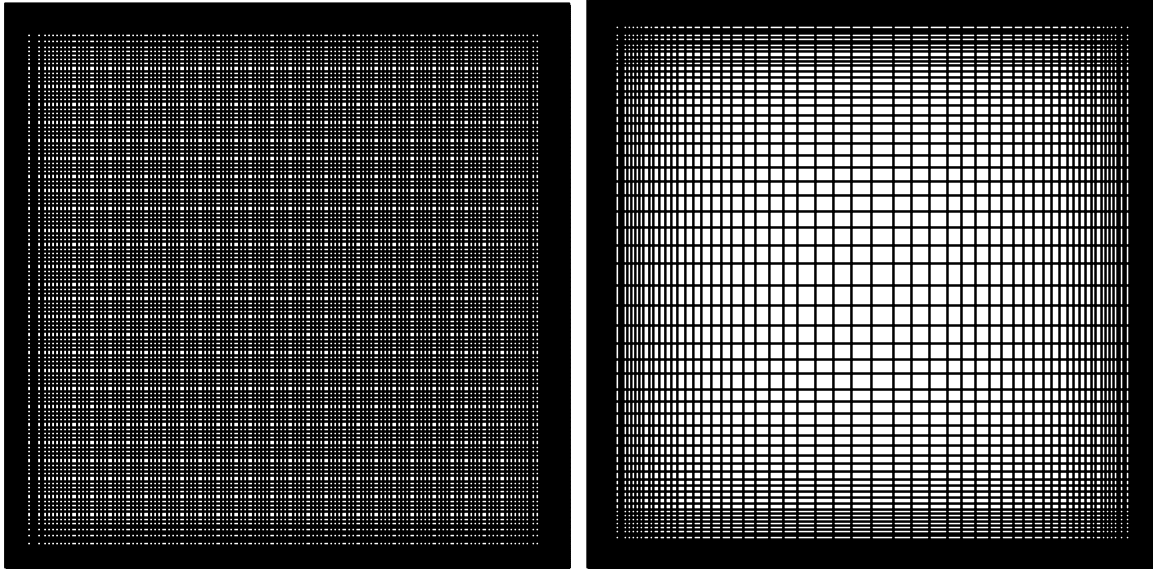


Figure 2. Example of two meshes: left, 160NU; right, 100 NU.

5. NEWTONIAN CALCULATIONS (ACCURACY)

Table 2 gives the vortex strength data obtained on consecutively refined uniform meshes for the Newtonian case with $Re = 0$. The order of convergence of the method obtained from the main recirculation intensity (counter clockwise vortex, thus the minimum streamfunction value, y_{\min} , is negative) is $p = 2.07$ in good agreement with the formal second-order accuracy of the differencing schemes employed. The vertical position of the main vortex, y_{\min} , is also given and is seen not to be affected by mesh refinement. For creeping flow ($Re = 0$) the mid, vertical line is a symmetry line, and the position of the main vortex centre is thus $x_{\min} = 0.5$. Two additional secondary recirculations are formed close to the two bottom corners of the cavity, see Fig. 5 below; these have a much smaller intensity compared to the main vortex, and its value is also given in Table 2 as y_{\max} .

Mesh	Δx	$y_{\min} (\times 10^{-2})$	y_{\min}	$y_{\max} (\times 10^{-6})$
50 U	0.02	-8.3494	0.780	3.1070
100 U	0.01	-8.3624	0.780	1.9431
200 U	0.005	-8.3655	0.780	1.7378

Table 2. Main and secondary vortex intensities for the Newtonian case ($Re = 0$)

Figure 3 shows the local variation near the singular corner ($x = 1$, $y = 1$) of the vertical normal stress t_{yy} as predicted by the method (rounded symbols) and the expected variation based on a theoretical solution by Taylor [8] (green line). Grid 3 having a non-uniform grid spacing with a $\Delta y_{\min} = 0.001$ allows better resolution close to the walls compared with a uniform grid with the double of cells along each direction (but $\Delta y_{\min} = 0.005$).

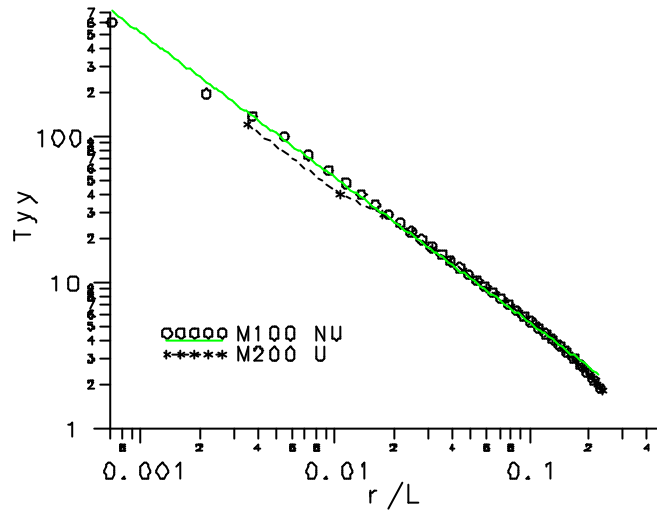


Figure 3. Asymptotic variation of the normal stress near the corner

The theoretical slope is -1 and the numerical data are fitted by a straight line with slope -0.99 thus demonstrating the quality of the predictions.

Theoretical values of tangential and normal velocity components at a line making an angle of 45° degrees to that corner are shown in Fig. 4 and compared with Taylor's solution [8]. This gives 0.216 for the tangential component and 0.266 for the normal component and as seen in Fig. 4 good agreement is achieved except for the last couple of points where, due to localised errors resulting from boundary conditions, the last predicted values deviate from the theoretical lines.

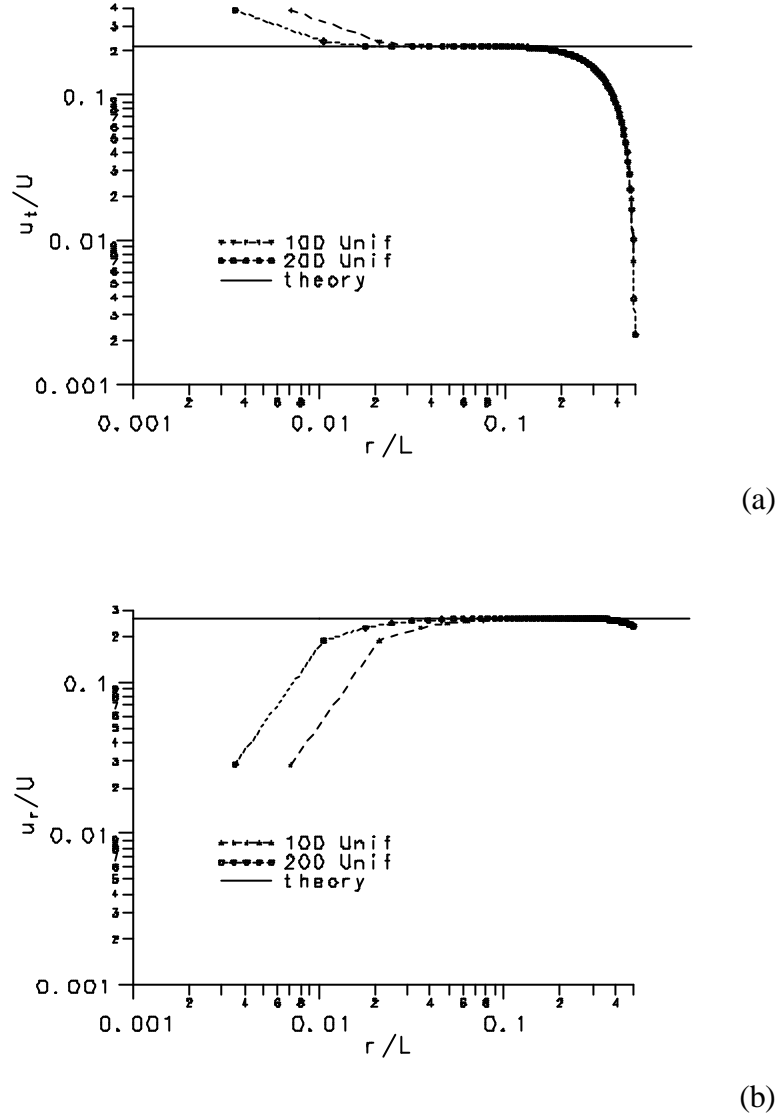


Figure 4. Asymptotic variation of the tangential (a) and radial (b) velocity components near the corner; lines show theory [8]: 0.216 and 0.266.

6. STEADY VISCOELASTIC CALCULATIONS

Streamlines based on creeping flow conditions for Newtonian ($De = 0$) and FENE-MCR ($De = 1$) viscoelastic cases are shown in Fig. 5. The former case is shown with solid lines and the latter by dashed lines, making it clear the upstream deviation of the main cavity vortex centre due to elasticity.

Experiments by Pakdel et al [1] illustrate in a practical situation this effect with photographic visualizations and in ref. [3] this upstream dislocation of the closed recirculating lines was demonstrated but only by a very small margin. This limitation occurred because the cavity in ref. [3] was not regularised in terms of the applied velocity variation, as we have done here, but rather by introducing a small leakage between the moving top wall and the two vertical side walls. With that method, the Deborah number could not be raised above around 0.25 .

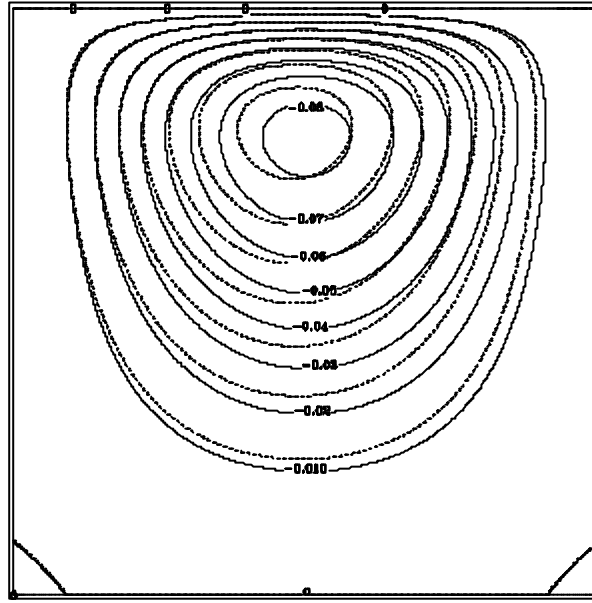


Figure 5. Comparison of streamlines for steady Newtonian (solid) and Viscoelastic ($De=1$, dashed) flows.

The amount of recirculating flow in the cavity, measured by the minimum stream function value, ψ_{\min} , is shown in Fig. 6 as a function of the Deborah number. This flow rate was made dimensionless by dividing by the top-wall velocity value U_w and the cavity height H , and, as seen in Fig. 6, the vortex strength is about 8.4%. In order to demonstrate mesh independence, results are shown for two meshes, with 100×100 and 160×160 CVs (Grids 3 and 4 of Table 1).

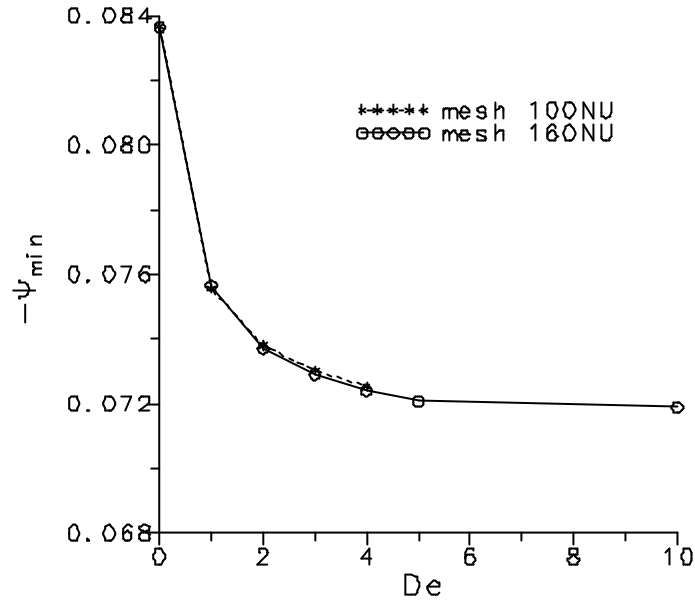


Figure 6. Variation of the main vortex strength with elasticity

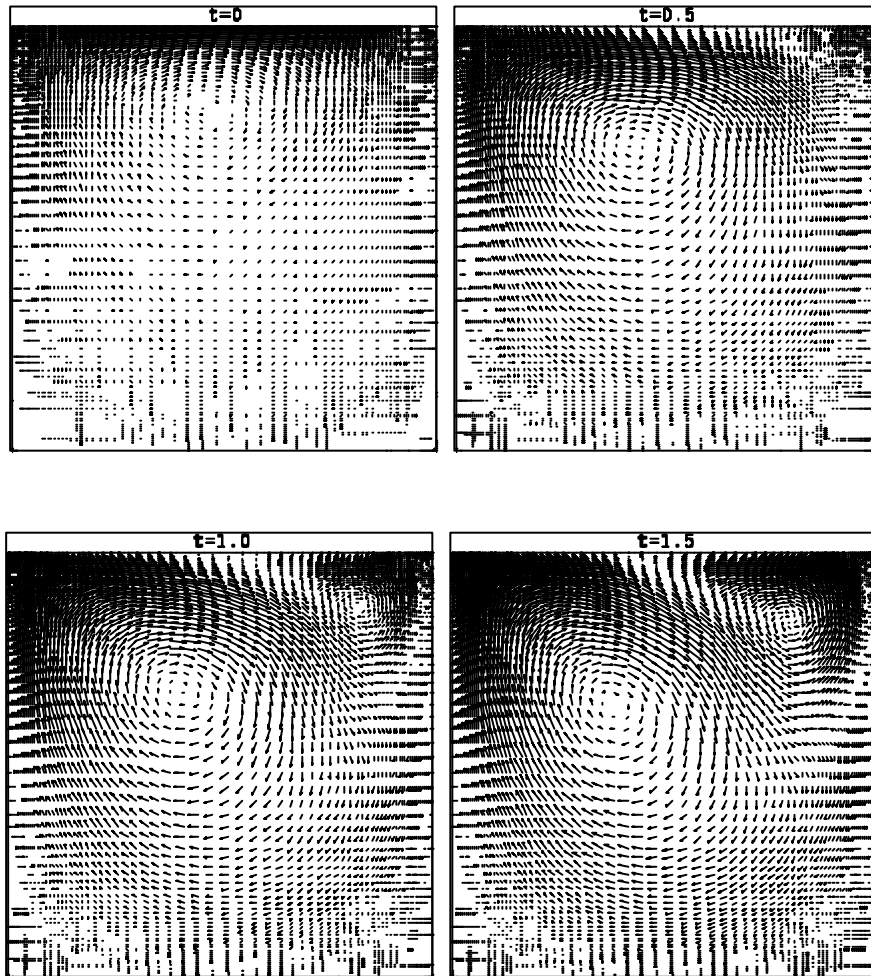
To serve as benchmark data, the values of the main vortex intensity and the position of its centre are also given under tabulated form in Table 3. Recall that these values are for the FENE-CR model (Eq. 4) with an extensibility parameter of $L^2 = 100$ and a solvent viscosity ratio of $\mathbf{b} = 0.79$.

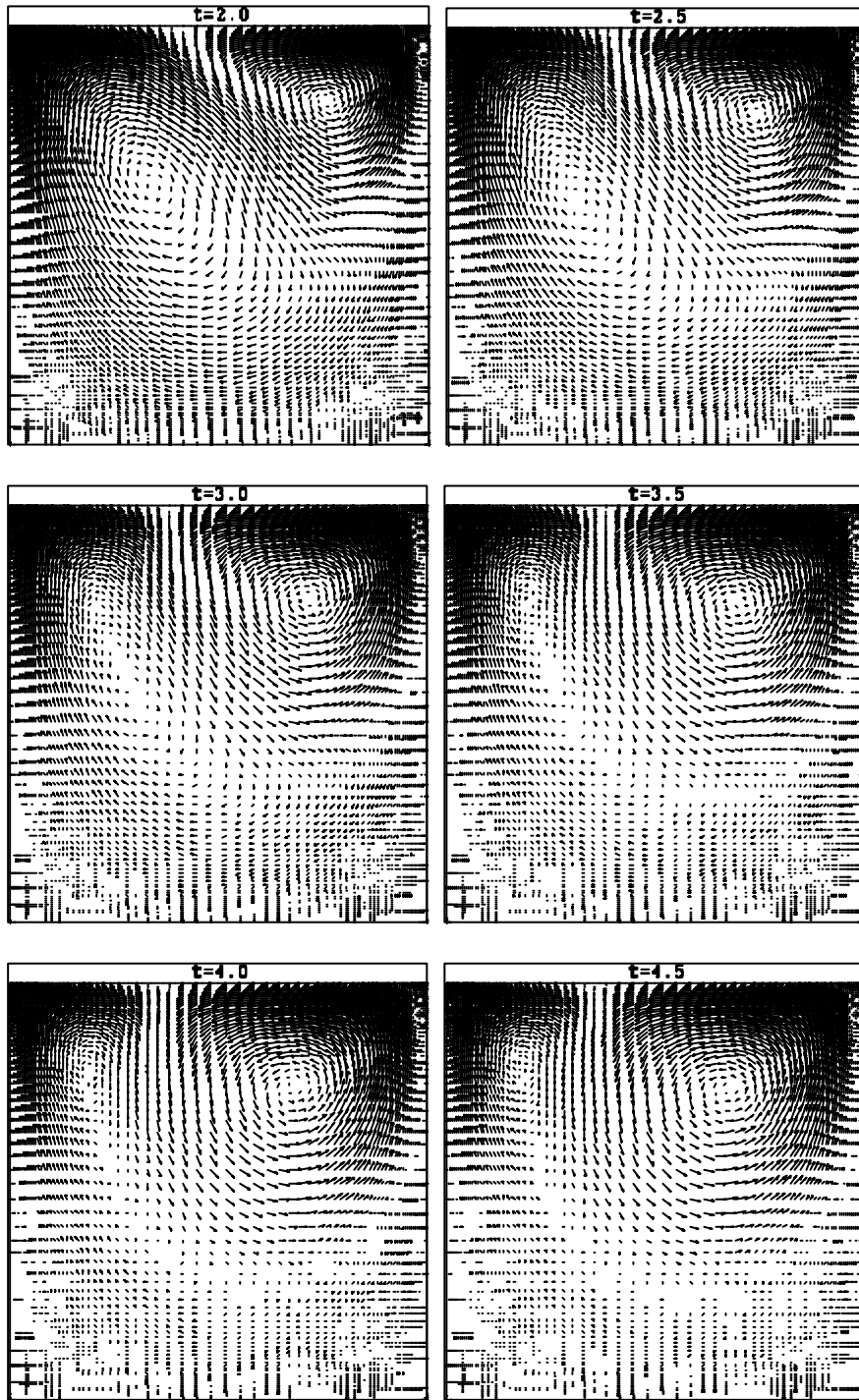
De	Grid 4, 160x160 NU			Grid 3, 100x100 NU		
	$-y_{\min} (\times 10^{-2})$	x_{\min}	y_{\min}	$-y_{\min} (\times 10^{-2})$	x_{\min}	y_{\min}
0	8.364	0.500	0.780	8.366	0.500	0.784
1	7.564	0.476	0.796	7.556	0.464	0.800
2	7.370	0.468	0.804	7.380	0.464	0.800
3	7.290	0.460	0.804	7.303	0.464	0.800
4	7.240	0.460	0.804	7.254	0.464	0.800
5	7.207	0.452	0.804			
10	7.189	0.452	0.804			

Table 3. Main vortex intensities and centre position for the viscoelastic cases ($Re = 0$)

7. UNSTEADY VISCOELASTIC CALCULATIONS (RECOIL)

Pakdel et al. [1] have shown in their experiments that a polymer solution suffers recoil after cessation of the top wall movement. Recoil is seen by a counter rotating recirculating motion, relative to the main vortex motion generated by the steady lid dragging prior to cessation, and may be explained by the elastic stretching and compression of the polymer molecules. In Fig. 7 this is illustrated by velocity vectors of the flow after stopping the lid of a steady viscoelastic case with $De = 4$. The numbers (should be multiplied by 10^{-2}) at the top of these figures refer to the time after flow cessation, which was assumed to occur at $t = 0$. A time step of $\Delta t = 0.5 \times 10^{-4}$ was employed for these simulations which were done on Grid 3.





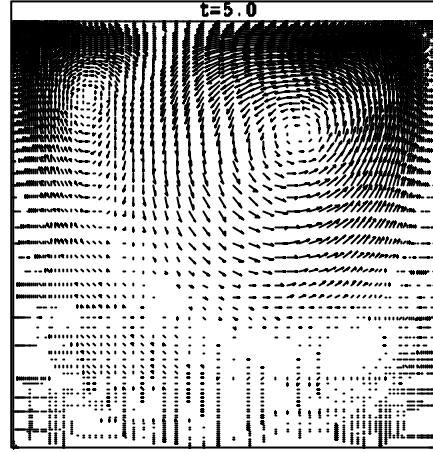


Figure 7. Velocity vector fields after cessation (at $t = 0$) of the lid movement (case $De = 4$; $t \times 10^{-2}$).

The next figure (Fig. 8) shows the decay of the maximum velocity in the cavity for inertialess flow ($Re = 0$), as predicted on Mesh 160x160 NU, for three Deborah numbers: $De = 0$ (Newtonian case); $De = 1$ and $De = 2$. The period of decay for the Newtonian case is 0.018 in terms of a non-dimensional time, while for the two viscoelastic cases the periods obtained from the simulations are 0.75 ($De = 1$) and 1.48 ($De = 2$). It can be observed from Fig. 8 that Pakdel et al's data follow a time decay in between the above values. When the periods of decay are scaled with the relaxation times, the experimental data of [1] give $T/I \approx 0.71$ (for the case with $I = 1.6$ s) while our predictions yield values of 0.75 (for $De = 1$) and 0.74 ($De = 2$).

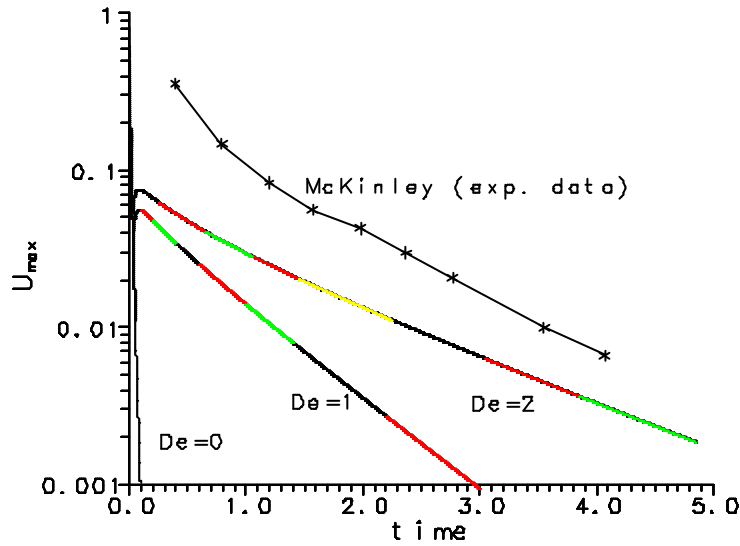


Figure 8. Time decay of the maximum velocity in the field for several flow cases.

In order to illustrate the parameters controlling the recoil process, Fig. 9 shows in a log-log scale the variation of the maximum velocity value in the cavity for three flow cases: Newtonian ($De = 0$), $De = 1$ and $De = 2$ (with FENE-CR). Clearly, at small times the process is controlled by the diffusion time scale, but for later times the relaxation time takes over and controls the rate of decay of the flow field in the cavity after cessation of the lid motion.

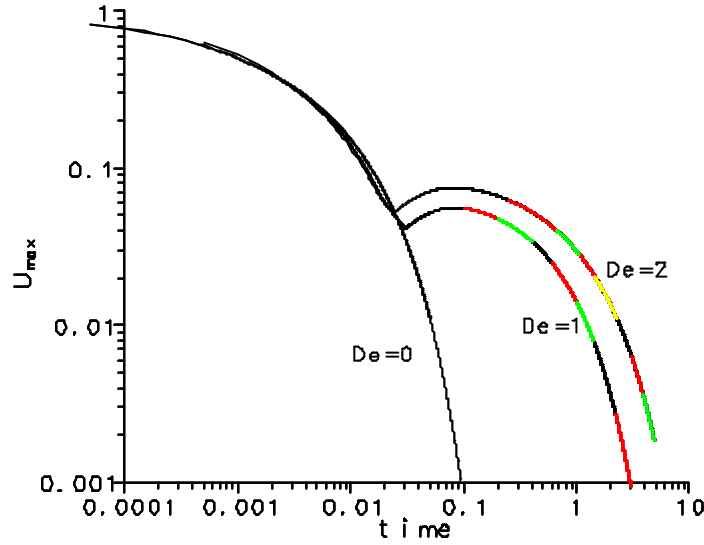


Figure 9. Log-scale variation of the maximum velocity decay: Newtonian and two viscoelastic cases.

8. CONCLUSIONS

The paper has presented results of the application of a finite volume method to the simulation of viscoelastic flows in a square cavity with a moving lid. The lid velocity was regularised by assuming a polynomial variation with vanishing values for velocity and its first derivative at the two corners. This regularisation allowed numerical solutions to be obtained at high Deborah numbers, in contrast to previous studies where De was typically below 0.3, without significantly altering the structure of the flow inside the cavity. Elasticity was found to influence the flow as in the experiments of Ref. [1]: the centre of the large cavity vortex is displaced upstream as De is raised; and the amount of recirculating fluid decreases when De is increased. The recoil phenomenon reported in Ref. [1] was

also well reproduced by the time dependent simulations: while for a Newtonian fluid the vortex decreases steadily and relatively quickly when the top wall is stopped, for the viscoelastic fluid the elastic energy stored during the initial period of steady lid motion is later released, leading to a counter-rotating vortex that eventually occupies the whole cavity. This time dependent phenomenon is illustrated with a sequence of velocity vector plots that clarify the origin of the new “recoil” vortex in the right top corner of the cavity, a zone where the polymer molecules were subject to high levels of compression during the preceding steady motion.

The results obtained can be usefully employed as benchmark data by other researchers that wish to consider this cavity flow as a test case in viscoelastic code development.

Acknowledgments

Project POCTI/48665/EME/2002 is gratefully thanked together with Fundação para a Ciência e Tecnologia (FCT, Portugal) and FEDER for funding this work.

REFERÊNCIAS

- [1] P. Pakdel, S.H. Spiegelberg, and G.H. McKinley, “Cavity flows of elastic liquids: Two-dimensional flows”, *Phy. Fluids*, **9**, 3123, (1997).
- [2] M. Renardy 2003. Stress integration for the constitutive law of the upper convected Maxwell fluid near the corners in a driven cavity. *J. Non-Newt. Fluid Mech.*, **112**, 77-84 (2003).
- [3] A.M. Grillet, B. Yang, B. Khomami, E.S.G. Shaqfeh, “Modeling of viscoelastic lid driven cavity flow using finite element simulations”, *J. Non-Newt. Fluid Mech.*, **88**, 99-131 (1999).
- [4] M.D. Chilcott, J.M. Rallison, "Creeping flow of dilute polymer solutions past cylinders and spheres", *J. Non-Newt. Fluid Mech.*, **29**, 381-432 (1988).
- [5] P.J. Oliveira, "Method for time-dependent simulations of viscoelastic flows: Vortex shedding behind cylinder", *J. Non-Newt. Fluid Mech.*, **101**, 113-137 (2001).
- [6] M.A. Alves, P.J. Oliveira e F.T. Pinho, “A Convergent and Universally Bounded Interpolation Scheme for the Treatment of Advection”, *Int. J. Num. Methods in Fluids*, **41**, 47-75 (2003).
- [7] O. Botella, "On the solution of the Navier-Stokes equations using Chebyshev projection schemes with third-order accuracy in time", *Comp. & Fluids.*, **26**, 107-116 (1997).
- [8] G.I. Taylor, “Similarity solutions of hydrodynamic problems”, in *Aeronautics and Astronautics*, Ed. Hoff and Vincenti, Pergamon Press, pp. 21-28 (1960).